Feasibility of glass-ceramic coatings on alumina prosthetic implants by airbrush spraying method

Francesco Baino*, Chiara Vitale-Brovarone

Institute of Materials Physics and Engineering, Applied Science and Technology Department, Politecnico di Torino, Corso Duca degli Abruzzi 24, 10129 Torino, Italy

*Corresponding author: F. Baino

Tel.: +39 011 090 4668

Fax: +39 011 090 4624

E-mail: francesco.baino@polito.it

Abstract

This work explores the feasibility of glass-derived coatings (SiO_2-CaO-Na_2O-Al_2O_3 system) on bioceramic devices of complex shape by a layer-wise slurry deposition using an airbrush spray gun. Specifically, glass-ceramic coatings with thickness in the 50-500 μm range were prepared on alumina curved substrates by airbrush spraying of glass-based aqueous suspensions followed by sintering. Investigations by scanning electron microscopy and micro-computed tomography revealed that, under appropriate optimization of slurry composition and spraying cycles, this technique is suitable to manufacture homogeneous and continuous coatings on model curved ceramic surfaces. It was observed that neither cracking nor delamination occurred at the interface between coating and substrate. *Ad-hoc* tensile tests were carried out by properly adapting the relevant ASTM standard to the specific case (curved geometry); the coating adhesion strength was found adequate (about 25 MPa) for biomedical applications. A simple model describing the

relationship between coating thickness and number of spraying cycles was also developed and proposed as a useful tool to improve the design and manufacturing of bioceramic coatings.

Keywords: Coating; Bioceramic; Deposition; Joint prosthesis.

1. Introduction

Biological fixation is defined as the process by which prosthetic components become firmly bonded to host bone by tissue on-grow or in-growth without the use of bone cement [1]. In this regard, the deposition of a bioactive coating on the surface of an implant has been shown to be a smart strategy to improve implant fixation to the surrounding tissue [2]. Over the last 25 years, a number of methods have been experimented to produce bioceramic coatings, including gravity-controlled deposition [3-5], sol-gel dipping [6], spin coating [7], plasma spraying [8], sputtering [9] and electrophoretic deposition [10]. Plasma sprayed hydroxyapatite (HA) coatings on metal implants were introduced in the mid 1980s, received FDA approval and were demonstrated to promote stronger bonding to bone in comparison with the loosely adherent layer of fibrous tissue at the implant interface in other cementless fixations; however, some controversies about their clinical use still linger on. The control of variables in plasma spraying is a complex issue and small changes of processing parameters can highly affect the properties of the final coating; furthermore, the high temperatures required by the process can induce HA decomposition into soluble calcium phosphate compounds undergoing undesired fast resorption *in vivo* [8,9,11]. Bioactive glasses have been proposed as a promising alternative to HA in the manufacturing of coatings on prosthetic implants due to their unique versatility in terms of processing and *in vivo* performance [4,6,7,12], which, in principle, can be finely adjusted by controlling their composition [13-15]. Although the literature has demonstrated that it is possible to deposit glass layers that retain bioactivity, a recurrent problem is the generation of large thermal stresses during processing that can cause cracking or

delamination of the coating. The solution to the problem requires the development of coating procedures and bioactive glasses/glass-ceramics with adequate thermal expansion coefficients and softening points.

The research work reported in this article was carried out in the framework of the European project "MATCh" (Monoblock acetabular cup with trabecular-like coating), that aims to explore the feasibility of an innovative single-piece acetabular cup for hip joint prosthesis [16]. As depicted in Fig. 1a, this bioceramic implant is constituted by three elements, i.e. a bioinert ceramic substrate that articulates directly with the (prosthetic) femur head, a bioactive trabecular coating (scaffold) that aims to promote implant osteointegration to the patient's pelvic bone, and a glass-derived interlayer with the aim of improving the adhesion between alumina substrate (cup) and trabecular coating (scaffold). The fabrication of such a device is a complex task that requires the development of suitable strategies to deposit the dense coating (interlayer) on the curved bioceramic substrate and, subsequently, to produce the trabecular layer in the form of a hemispherical shell. The present work addresses to the first of these two challenges, investigating the feasibility of a glass-derived coating by airbrush spraying of SiO_2-CaO-Na_2O-Al_2O_3 (SCNA) glass powder suspensions followed by thermal treatment. Airbrush spraying of ceramic slurries is a versatile method that allows the coating of substrates having complex shape with an adequate control of coating thickness [17-20]; however, there is a paucity of studies about its use in the field of bioceramics. Very recently, Pardun et al. reported the characterization of wet nanopowder-sprayed zirconia/HA composite coatings on dental implants (screws) [21]. To the best of the authors' knowledge, the use of airbrush spraying on orthopaedic implants has been never documented and, accordingly, the present article represents a pilot study. The challenge behind this work, schematically illustrated in Fig. 1b, was to develop a reproducible and relatively easy method to coat ceramic prosthetic components having curved shape with a glass layer [22].

2. Materials and methods

2.1. Samples preparation

The model curved substrates to be coated were obtained by cutting high-purity (> 99 wt.%) alumina crucibles in sectors (length of the external arc: 40 mm; external radius: 19 mm; wall thickness: 2.9 mm; width: 10 mm) using a diamond blade (Accutom 5, Struers). Before treatment the curved alumina substrates were washed with deionized water and acetone; the surface of the specimens was not abraded.

The material used for coating preparation was a silicate quaternary glass with the following molar composition: $57SiO_2$-$34CaO$-$6Na_2O$-$3Al_2O_3$ (SCNA) [22,23]. The glass reagents (high-purity powders of SiO_2, $CaCO_3$, Na_2CO_3 and Al_2O_3 purchased from Sigma-Aldrich) were molten in a platinum crucible at 1550 °C for 1 h in air; the melt was quenched in cold water to obtain a frit, that was subsequently ground by a 6-balls zirconia milling machine and sieved (stainless steel sieves, Giuliani Technologies Srl) to a final particle size below 32 μm. Preliminary experiments showed that the use of glass powder with higher particle size for slurry preparation resulted in an enhanced risk of blocking the nozzle of the airbrush system.

Different SCNA-based slurries were produced from SCNA powder, water and, optionally, additives as reported in Table 1. Poly(vinyl alcohol) (PVA) was used as a binder; glycerine was introduced as an additive in the attempt to ensure a more uniform drying. All slurries were prepared under continuous magnetic stirring at 300 rpm. As to slurries D and E, glass powder was added after PVA hydrolysis. Glycerine was introduced into the slurries C and E together with glass powder. After the addition of glass powder, the slurries were always stirred at 300 rpm for 15 min to ensure homogeneity and then the layer-wise slurry deposition on the alumina substrates was performed by an airbrush spray gun (Evolution Silverline M, Harder & Steenbeck, Germany); by its double-action trigger, the addition of slurry and compressed air (AirCom Eolo 30 compressor, Italy) was individually controlled. The quantity of the spraying mixture was kept steady by controlling the

spray pressure (3.5×10^5 Pa) and the optimal spray total time (2 s) selected on the basis of preliminary experiments. A schematic view of the process of slurry deposition by airbrush is reported in Fig. 2.

Single green layers were dried at room temperature for 1 h at the end of each spraying cycle. Once all the depositions were completed, the samples were dried overnight under ambient conditions and subseequently thermally treated in an electrical furnace at 1000 °C for 3 h (heating and cooling rates were set at 5 and 10 °C min^{-1}, respectively).

2.2. Samples characterization

As-poured SCNA powder and thermally-treated SCNA-derived coatings underwent wide-angle X-ray diffraction (XRD; 2θ within 10-70°) to assess the presence of crystalline phases. The analyses were performed by using a X'Pert diffractometer (Philips) operating at 40 kV and 30 mA with Bragg-Brentano camera geometry, Cu Kα incident radiation (wavelength λ = 0.15405 nm), step size Δ(2θ) = 0.02° and fixed counting time of 1 s per step. Crystalline phases were identified by using X'Pert HighScore program equipped with PCPDFWIN database.

The samples were embedded in epoxy resin (Epofix, Struers), cut and polished using #600 to #4000 SiC grit paper; the obtained cross-sections were metal-coated and then analysed by scanning electron microscopy (SEM, Philips 525 M; working voltage: 15 kV) to evaluate the quality of the coating. Compositional investigations were performed by energy dispersive spectroscopy (EDS; Philips EDAX 9100).

The coatings were non-destructively investigated by micro-computed tomography (micro-CT; SkyScan 1174, Micro Photonics Inc.). For this experiment the source voltage and current were 50 kV and 800 μA, respectively, with a sample-to-detector distance of 40 mm; the resulting voxel size was 9 μm × 9 μm × 9 μm; the exposure time was set to 8 s per projection. The reconstruction of the tomographic slices was carried out using the software N-Recon applying the standard filtered back-

projection algorithm. Visualization of the complete 3-D reconstruction of the sample was performed using the software CT-Vox.

The adhesion strength of SCNA coatings was assessed following the relevant ASTM standard [24], under an appropriate adaptation for the curved samples to mimic a "nearly-flat" case. SCNA-coated curved alumina samples were cut in smaller pieces (approximately 10 mm × 10 mm) and glued to two loading fixtures (16-mm diameter steel cylinders to be connected to the testing machine by metal pins) using an epoxy resin (Araldite® AV 119, Ciba-Geigy), which is able to withstand a maximum tensile stress of about 40 MPa (as declared by the manufacturer). At room temperature the adhesive was a gel and its polymerization was achieved by a low-temperature treatment in oven (140 °C for 1 h). As the SCNA-coated samples were characterized by a certain curvature, the maintenance of fixtures coaxiality was a crucial issue to obtain reliable results. Due to the absence of indications in existing literature, we developed an *ad-hoc* tool with circular guides matching the fixtures size and allowing coaxiality upon resin hardening, in order to avoid misalignment problems. The adhesion strength of the coatings was assessed by applying tensile loads to the samples (Syntech 10/D machine, MTS Corp.; cross-head speed of 1 mm min^{-1}) and calculated as L_t / A_t , wherein L_t (N) is the failure tensile load and A_t (mm^2) is the area on which the load was applied. SCNA coatings on flat alumina substrates (10 mm × 9 mm × 1 mm) were also prepared and mechanically tested under the same experimental conditions for the purpose of comparison The data were expressed as mean value ± standard deviation calculated on five samples.

3. Results and discussion

As-poured SCNA was a completely amorphous material (glass), as demonstrated by the broad halo (2θ within 20-35°) in the XRD pattern shown in Fig. 3a. One crystalline phase, identified as wollastonite ($CaSiO_3$, PDF code: 00-027-0088), was detected in the thermally-treated coatings (Fig. 3b); this phase is known to be highly biocompatible and suitable for applications in the biomedical

field [25,26]. This finding is consistent with previous studies by the authors, who reported the development of this phase after thermal treatment of SCNA above 900 °C [22,27,28]. Therefore, it should be taken into account that the sintered SCNA constituting the coating is actually a glass-ceramic material; however, for purpose of simplicity it will be hereafter adopted the expression "SCNA coating", without further specifying its glass-ceramic nature.

As demonstrated in previous works by the authors, sintered SCNA is characterized by a nearly inert behaviour in a biological environment [22]. In the context of bone tissue engineering, the term "bioactivity" refers to the property of some biomaterials, e.g. bioactive glasses, to be coated by a surface apatite layer both *in vitro* and *in vivo*, which is possible due to a sequence of ion exchange phenomena occurring between implant and biological fluids [29]. In the case of SCNA-derived glass-ceramic, the partial substitution of Si^{4+} with Al^{3+} in the tetrahedral $(SiO)^{4-}$ units of the Al_2O_3-rich residual glass phase of sintered SCNA led to a chemically stable network less prone to react with the biological environment [22]; these results were consistent with the observations reported by Kokubo and co-workers for Al_2O_3- and wollastonite-containing glass-ceramics [30]. It is worth underlining that high chemical stability of the coating is a key property in view of the application illustrated in Fig. 1a, where the SCNA interlayer should act as a joining element between alumina substrate and bioactive trabecular coating.

Continuous coatings with quite homogeneous thickness were produced using the slurry A (Figs. 4a-d) but, due to the high solid content (50 wt.% glass), an accelerated drying process was observed, which represents an undesired effect resulting in two kinds of problems. First, partial delamination at the interface occurred (Figs. 4a and c): during the drying process, the built-up layer bent upwards at its perimeter, and since the adhesion of the single layers proved superior to the adhesion between the green body and the substrate [20], the green body was separated from the substrate. Furthermore, the high solid content caused an enhanced risk of blocking the nozzle of the airbrush system, which involved serious problems from a technological viewpoint. It was also noted that an increase of the coating thickness was associated to a higher number of defects (pores or cracks) in

the coating, due to entrapment of air between the single green layers produced with each spraying cycle (Figs. 4b and d).

In order to solve these problems, the solid content was decreased to 30 wt.% (slurry B); by doing so, however, the drying process was too slow and coatings with inhomogeneous thicknesses were obtained (Figs. 4e-h). Due to gravity, the slurry tended to accumulate at the ends of the alumina substrate following its curvature, thereby causing the thinning of the coating in the central region. The air bubbles tended to coalesce forming large spheroidal cavities in the thicker regions of the coating, i.e. at the ends of the curved alumina substrate (Fig. 4h).

Glycerine was then introduced in the slurry formulation (slurry C) in the attempt to ensure a more uniform drying [20]; this strategy, however, was unsuccessful since a combination of the specific problems already noticed for slurries A (Fig. 5a) and B (Fig. 5b) was observed (slurry accumulation at the substrate ends and presence of defects at the coating/substrate interface).

Substitution of glycerine with PVA as a binder (slurry D) led to significantly better results: continuous coatings with quite homogeneous thickness along the cross-sectional profile of the curved alumina substrate were obtained, without cracks or delamination at the interface with the substrate (Figs. 5c-f). Few closed pores inside the coating can be observed due to air entrapment occurring during the airbrush spraying. The amount and size of longitudinal, elongated pores roughly parallel to the interface increased dramatically with the increment of the coating thickness, i.e. with the number of spraying cycles (Figs. 5g and h). Their presence was due to air entrapment between adjacent layers deposited with subsequent spraying cycles; furthermore, PVA burn-off during the thermal treatment was accompanied by development of gases that accumulated in these cavities, thus causing local swelling and tensile stresses in the coating. Since the adhesion of the single layers proved superior to the adhesion between the green coating and the substrate [20], coating lift-up at the ends of the samples can occur (Fig. 5g). In the case of relatively thin coatings (around 100-150 μm), the gas can more easily diffuse out of the material during the thermal treatment and, accordingly, these problems were less significant (Figs. 5c-f).

Combined use of PVA and glycerine with a high solid load (slurry E) led to unsatisfactory results (Fig. 6): even in case of coatings produced with a low number of spraying cycles, the presence of elongated pores in the coating was important; with respect to the slurry D, this phenomenon was probably emphasized due to the burn-off of a higher amount of organic matter (PVA and glycerine) upon heating.

As a general remark, it is worth underlining that, except for some specific problems related to slurry formulation (e.g. the large interfacial defects visible in Figs. 4a and c), the quality of adhesion between SCNA coating and alumina substrate after thermal treatment is generally very good; this is due to the good matching between the thermal expansion coefficients of alumina (8.5×10^{-6} $°C^{-1}$) and SCNA (8.7×10^{-6} $°C^{-1}$) [22,27,28]. In this regard, Fig. 7 qualitatively shows an excellent adhesion between the two materials, without interfacial crack or flaws. The glass-ceramic nature of the SCNA coating is also visible in Fig. 7, where "white" crystals of $CaSiO_3$ (the phase identification is reported in Fig. 3b) can be clearly detected, in good agreement with previous findings by the authors [22].

Micro-CT is an advanced characterization technique that, when combined with 3-D image analysis, can provide both qualitative and quantitative information on biomaterials; in recent years, it has been often employed for the non-destructive investigation of porous structures of biomedical interest, such as cancellous bone and tissue engineered scaffolds [31-33]. In the present work, micro-CT was interestingly used to assess whether a continuous SCNA coating was actually deposited on the whole curved surface of the alumina substrate by airbrush spraying; this investigation, performed in a 3-D space, is complementary to SEM analyses that provide information on a single 2-D cross-section of the sample. A typical 3-D reconstruction of a SCNA-coated sample (slurry D, 10 spraying cycles) is shown in Fig. 8a. The two materials constituting the sample (alumina and SCNA) can be easily discriminated by further post-processing with the software CT-Vox, that enables to assign different colours to materials with different densities (the densities of alumina and SCNA are 4.0 and 2.7 g cm^{-3}, respectively). Fig. 8a shows that the SCNA

layer continuously and homogeneously coats the whole curved substrate lying underneath, thereby demonstrating the effectiveness of the proposed method to apply coatings on objects having complex, curved shape. The SCNA coating alone ("separated" from the alumina substrate) is also visualized in Fig. 8b. Looking at Fig. 8a, a grey-green transition zone can be distinguished at the interface between alumina and SCNA coating, which could be originated from the interfacial atomic diffusion upon the thermal treatment. This hypothesis seems to be confirmed by EDS analysis (Fig. 9), in good agreement with previous observations carried out in flat geometry [22].

In order to obtain quantitative data, SCNA coatings produced with 10 airbrush spraying cycles using the slurry D (mean thickness around 150 μm) were selected as the most promising ones (few small closed pores, without the risk of resin infiltration inside the coating) and used for tensile tests. The adhesion strengths of the coatings deposited on curved and flat substrates were 29.7 ± 4.7 MPa and 21.5 ± 5.0 MPa, respectively; an example of fracture area is reported in Fig. 10. The adhesion strength of the coating is not negatively affected by the shape of the substrate (curved vs. flat surface), which further confirms the versatility of airbrush spraying method to produce coatings from glass powder suspensions. If we refer to international standards, a tensile stress of at least 15 MPa is recommended in the case of HA coatings on surgical implants [34]; therefore, the adhesion strength obtained for the airbrush sprayed SCNA coatings suggests the mechanical suitability of the prepared material for biomedical use.

The major aim of the present work was to investigate whether the airbrush spraying method could be successfully applied to coat curved ceramic substrates starting from glass powder suspensions, and our preliminary results are promising. However, it is worth mentioning that the alumina crucible used in this study is a model curved substrate that only roughly mimic the alumina commercially produced for medical applications. Further investigations will allow to draw more definite conclusions about the mechanical reliability of these coatings on implantable devices.

As closing remarks, a few considerations about the relationship between coating thickness (t) and number of airbrush spraying cycles (N) are presented by the authors, also in view of the process up-

scaling from “Lab research level” to industrial application. SEM and micro-CT investigations revealed that, from a general viewpoint, the value of t increases with the increment of N. In this study some important processing variables such as air pressure, nozzle diameter, velocity of the spraying movement and distance from nozzle to substrate (Fig. 3b) were kept constant. Hence it is possible to assume that, for the same slurry composition and maintaining constant the above mentioned parameters, the coating thickness is only dependent on the number of spraying cycles. Therefore, the coating thickness t can be related to N by means of a mathematical function with the initial condition t(N = 0) = 0. A simple first-order polynomial function, t = CN, was used for the interpolation; the model constants C as well as the correlation coefficients R^2 are reported in Table 2. Comparison among the fitting curves and the experimental data is reported in Figure 9. Fitting results generally exhibit good agreements with experimental data, as demonstrated by the high values of the coefficients R^2, which also reveals the good predictive capability of the presented approach. It is possible to observe that, under the same number of spraying cycles, the coating thickness increases with the increment of the glass content in the slurry (slurry E > slurries B and D). As already observed in Figs. 4e-h, the thickness of the coatings produced with the slurry B is significantly lower in comparison with those of the other sample batches, due to the absence of the binding agent (PVA) and the relevant problems of green layer removal by the subsequent spray cycles.

The obtained interpolating functions can be a valuable tool at the designer’s disposal to link the thickness of final coating with one of the key processing parameters – the number of spraying cycles, N – that can be easily controlled during the coating manufacture. In this regard, the analytical model describing the t-N relationship can be successfully employed for a “predictive purpose” and not only in a “descriptive way”: in fact, knowing the coating thickness recommended or, in general, suitable for a given application, it is possible to purposely control the number of spraying cycles so that the coating can fulfil the desired requirement. This strategy would allow to avoid unwanted loss of experimental time for samples preparation and subsequent checking – which

is unavoidably associated to the conventional "trial-and-error" approach – and could be easily implemented on production lines for the industrial manufacturing of bioceramic coatings.

4. Conclusions

Airbrush spraying method was innovatively used to produce biomedical glass-ceramic coatings on model alumina substrates with curved shape. The coatings were prepared by sequentially spraying glass-based aqueous suspensions containing PVA or glycerine as additives in appropriate amounts. Under careful set-up of slurry composition and number of spraying cycles, this technique of deposition proved to be suitable for obtaining continuous glass-derived coatings with homogeneous thickness on bioceramic product of complex shape. The adhesion strength of the coating to the model substrate (around 30 MPa), assessed by *ad-hoc* designed tensile tests, overpasses by two times the minimum threshold value recommended by ASTM standards for bioceramic coatings, which suggests the material suitability for biomedical use. Simple analytical models describing the relationship between coating thickness and number of spraying cycles were also proposed. The models can be used in a "direct way" to predict the coating thickness using the number of spraying cycles as a model input, but they can be also interestingly employed in an "inverse way": using the thickness as an input, the coating designer can obtain the number of spraying cycles needed to reach the desired thickness, thereby exploiting the model as a useful tool at the manufacturing stage.

Acknowledgements

This work was supported by the EU-funded project MATCh ("Monoblock acetabular cup with trabecular-like coating", Grant no. 286548).

References

[1] W.L. Jaffe, D.F. Scott, Current concepts review: total hip arthroplasty with hydroxyapatite-coated prostheses, J. Bone Joint Surg. 78 (1996) 1918-1934.

[2] Y. Ramaswamy, C. Wu, H. Zreiqat, Orthopaedic coating materials: considerations and applications, Expert Rev. Med. Devices 6 (2009) 423-430.

[3] S. Lopez-Esteban, E. Saiz, S. Fujino, T. Oku, K. Suganuma, A.P. Tomsia, Bioactive glass coating for orthopaedic metallic implants, J. Eur. Ceram. Soc. 23 (2003) 2921-2930.

[4] C. Vitale-Brovarone, E. Verné, SiO_2-CaO-K_2O coatings on alumina and Ti6Al4V substrates for biomedical applications, J. Mater. Sci.: Mater. Med. 16 (2005) 863-871.

[5] A. Bigi, E. Boanini, B. Bracci, A. Facchini, S. Panzavolta, F. Segatti, L. Sturba, Monocrystalline hydroxyapatite coatings on titanium: a new fast biomimetic method, Biomaterials 26 (2005) 4085-4089.

[6] M.H. Fathi, A. Doostmohammadi, Bioactive glass nanopowder and bioglass coating for biocompatibility improvement of metallic implant, J. Mater. Processing Technol. 209 (2009) 1385-1391.

[7] X. Wang, X. Li, K. Onuma, A. Ito, Y. Sogo, K. Kosuge, A. Oyane, Mesoporous bioactive glass coatings on stainless steel for enhanced cell activity, cytoskeletal organization and AsMg immobilization, J. Mater. Chem. 20 (2010) 6437-6445.

[8] L. Sun, C.C. Berndt, K.A. Gross, A. Kucuk, Material fundamentals and clinical performance of plasma-sprayed hydroxyapatite coatings: a review, J. Biomed. Mater. Res. (Appl. Biomater.) 58 (2001) 570-592.

[9] Y. Yang, K.H. Kim, J.L. Ong, A review on calcium phosphate coatings produced using a sputtering process – an alternative to plasma spraying, Biomaterials 26 (2005) 327-337.

[10] A.R. Boccaccini, S. Keim, R. Ma, Y. Li, I. Zhitomirsky, Electrophoretic deposition of biomaterials, J. R. Soc. Interface 7 (2010) S581-S613.

[11] D.E. Steflik, Hydroxylapatite coatings on dental implants: benefits and risks, J. Oral Implantol. 20 (1994) 198-200.

[12] A.P. Tomsia, E. Saiz, J. Song, C.R. Bertozzi, Biomimetic bonelike composites and novel bioactive glass coatings, Adv. Eng. Mater. 7 (2005) 999-1004.

[13] L.L. Hench, Glass and medicine, Int. J. Appl. Glass Sci. 1 (2010) 104-117.

[14] F. Baino, C. Vitale-Brovarone, Three-dimensional glass-derived scaffolds for bone tissue engineering: current trends and forecasts for the future, J. Biomed. Mater. Res. A 97 (2011) 514-535.

[15] J.R. Jone, Review of bioactive glass: from Hench to hybrids, Acta Biomater. 9 (2013) 4457-4486.

[16] E. Verné, C. Vitale-Brovarone, L. Robiglio, F. Baino. Single-piece ceramic prosthesis elements. Patent no. WO 2008/146322 A2 (2008).

[17] A. Ruder, H.P. Buchkremer, H. Jansen, W. Mallener, D. Stoever, Wet powder spraying - a process for the production of coatings, Surf. Coatings Technol. 53 (1992) 71-74.

[18] C.E.P. Willoughby, J.R.G. Evans, The preparation of laminated ceramic composites using paint technology, J. Mater. Sci. 31 (1996) 2333-2337.

[19] R. Polanco, P. Miranzo, M.I. Osendi, Fabrication and microstructure of a ZrO_2-Ni functionally graded bonding interlayer using the airbrush spraying method, Acta Mater. 54 (2006) 2215-2222.

[20] A.M. Waetjen, D.A. Polsakiewicz, I. Kuhl, R. Telle, H. Fischer, Slurry deposition by airbrush for selective laser sintering of ceramic components, J. Eur. Ceram. Soc. 29 (2009) 1-6.

[21] K. Pardun, L. Treccani, E. Volkmann, G. Li Destri, G. Marletta, P. Strecbein, C. Heiss, K. Rezwan, Characterization of wet powder-sprayed zirconia/calcium phosphate coating for dental implants, Clin. Implant. Dent. Relat. Res. In press. DOI: 10.1111/cid.12071

[22] C. Vitale-Brovarone, F. Baino, F. Tallia, C. Gervasio, E. Verné, Bioactive glass-derived trabecular coating: a smart solution for enhancing osteointegration of prosthetic elements, J. Mater. Sci.: Mater. Med. 23 (2012) 2369-2380.

[23] F. Baino, C. Vitale-Brovarone, Mechanical properties and reliability of glass-ceramic foam scaffolds for bone repair, Mater. Lett. 118 (2014) 27-30.

[24] ASTM C633. Standard test method for adhesion or cohesion strength of thermal spray coatings. 2008.

[25] T. Kokubo, S. Ito, S. Sakka, T. Yamamuro, Formation of a high-strength bioactive glass-ceramic in the system MgO-CaO-SiO_2-P_2O_5, J. Mater. Sci. 21 (1986) 536-540.

[26] W. Xue, X. Liu, X.B. Zheng, C. Ding, In vivo evaluation of plasma-sprayed wollastonite coating, Biomaterials 26 (2005) 3455-3460.

[27] Q. Chen, F. Baino, N.M. Pugno, C. Vitale-Brovarone, Bonding strength of glass-ceramic trabecular-like coatings to ceramic substrates for prosthetic applications, Mater. Sci. Eng. C 33 (2013) 1530-158.

[28] H. Ma, F. Baino, S. Fiorilli, C. Vitale-Brovarone, B. Onida, Al-MCM-41 inside a glass-ceramic scaffold: a meso-macroporous system for acid catalysis, J. Eur. Ceram. Soc. 33 (2013) 1535-1543.

[29] T. Kokubo, H. Takadama, How useful is SBF in predicting in vivo bone bioactivity?, Biomaterials 27 (2006) 2907-2915.

[30] T. Kokubo, H. Kushitani, C. Ohtsuki, S. Sakka, T. Yamamuro, Effects of ions dissolved from bioactive glass–ceramics on surface apatite formation, J. Mater. Sci.: Mater. Med. 4 (1993) 1-4.

[31] S.R. Stock, Recent advances in X-ray microtomography applied to materials, Int. Mater. Rev. 53 (2008) 129-181.

[32] J.R. Jones, R.C. Atwood, G. Poologasundarampillai, S. Yue, P.D. Lee, Quantifying the 3D macrostructure of tissue scaffolds, J. Mater. Sci.: Mater. Med. 20 (2009) 463-471.

[33] C. Renghini, A. Giuliani, S. Mazzoni, F. Brun, E. Larsson, F. Baino, C. Vitale-Brovarone C, Microstructural characterization and in vitro bioactivity of porous glassceramic scaffolds for bone regeneration by synchrotron radiation X-ray microtomography, J. Eur. Ceram. Soc. 33 (2013) 1553-1565.

[34] ISO 13779-4. Implants for surgery – Hydroxyapatite - Part 4: Determination of coating adhesion strength. 2002.

Figure legends

Fig. 1. The concepts behind the research work presented in this article: (a) drawing of the innovative acetabular cup for hip joint prosthesis proposed by the authors in the framework of the EU-funded project "MATCh"; (b) schematic picture of the SCNA-coated curved bioceramic substrate investigated in this article.

Fig. 2. Overview of the glass coating deposition by airbrush: (a) summary of the 4-stage process; (b) experimental set-up (the coating was applied by a double-action airbrush from a distance of 100 mm and with an air pressure of 3.5×10^5 Pa; the airbrush nozzle diameter was 0.40 mm).

Fig. 3. XRD patterns of (a) as-poured SCNA and (b) SCNA-derived coating (thermal treatment at 1000 °C for 3 h)

Fig. 4. SEM micrographs of thermally-treated selected coatings produced using two-component slurries: (a) and (b) slurry A with 3 airbrush spraying cycles; (c) and (d) slurry A with 5 airbrush spraying cycles; (e) and (f) slurry B with 5 airbrush spraying cycles; (g) and (h) slurry B with 10 airbrush spraying cycles.

Fig. 5. Images of selected coatings produced using three-component slurries: (a) green coating and (b) thermally-treated coating produced using the slurry C with 5 airbrush spraying cycles; (c,d) regions near to one of the sample ends and (e,f) central region of a sintered coating obtained using the slurry D with 10 airbrush spraying cycles; (g) one of the sample ends and (h) central region of a sintered coating obtained using the slurry D with 15 airbrush spraying cycles.

Fig. 6. SEM micrographs of thermally-treated selected coatings produced using the four-components slurry (slurry E): (a) and (b) 3 airbrush spraying cycles; (c) and (d) 6 airbrush spraying cycles.

Fig. 7. High-magnification SEM picture showing the interface between SCNA coating and alumina curved substrate.

Fig. 8. Micro-CT analysis on a typical SCNA coating produced by airbrush spraying of slurry D (10 spraying cycles) on curved alumina (post-processing of the images was performed with the software CT-Vox): (a) 3-D reconstruction of a large portion of the sample where the two constituent materials are discriminated using a colour code (alumina substrate = grey, SCNA coating = green); (b) visualization of the SCNA coating without the alumina substrate.

Fig. 9. Elemental line profiles for Al, Si, Ca and Na in the alumina substrate/SCNA coating interfacial area.

Fig. 10. Fracture area of SCNA coating (curved geometry) after tensile test.

Fig. 11. Relationship between coating thickness (t) and number of spraying cycles (N) for the coatings produced with different slurries (the dashed lines correspond to the linear fitting of the experimental data; the model parameters are reported in Table 2).

Tables

Table 1. Compositions and labelling of the slurries.

	Composition (wt.%)			
Slurry	SCNA powder	Water	PVA	Glycerine
A	50	50	-	-
B	30	70	-	-
C	30	64	-	6
D	30	64	6	-
E	50	40	3	7

Table 2. Modelling of the relationship between coating thickness (t) and number of spraying cycles (N) through linear fitting (t = CN): model constants and coefficients of determination.

Slurry	C (μm)	R^2
Slurry B	3.686	0.93
Slurry D	27.160	0.92
Slurry E	28.023	0.89

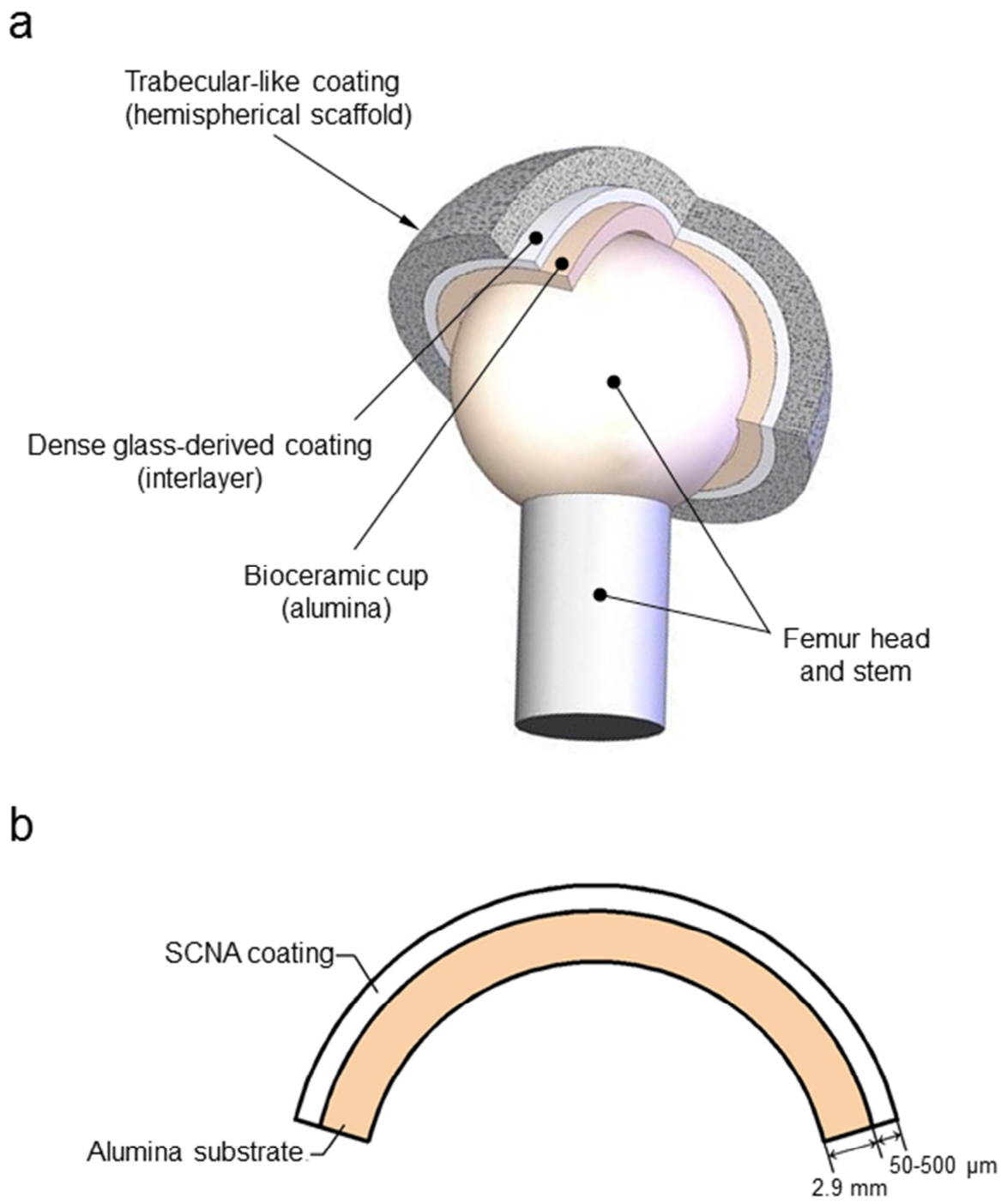
a
Trabecular-like coating
(hemispherical scaffold)
Dense glass-derived coating
(interlayer)
Bioceramic cup
(alumina)
Femur head
and stem
b
SCNA coating
Alumina substrate
50-500 µm
2.9 mm

Fig. 1

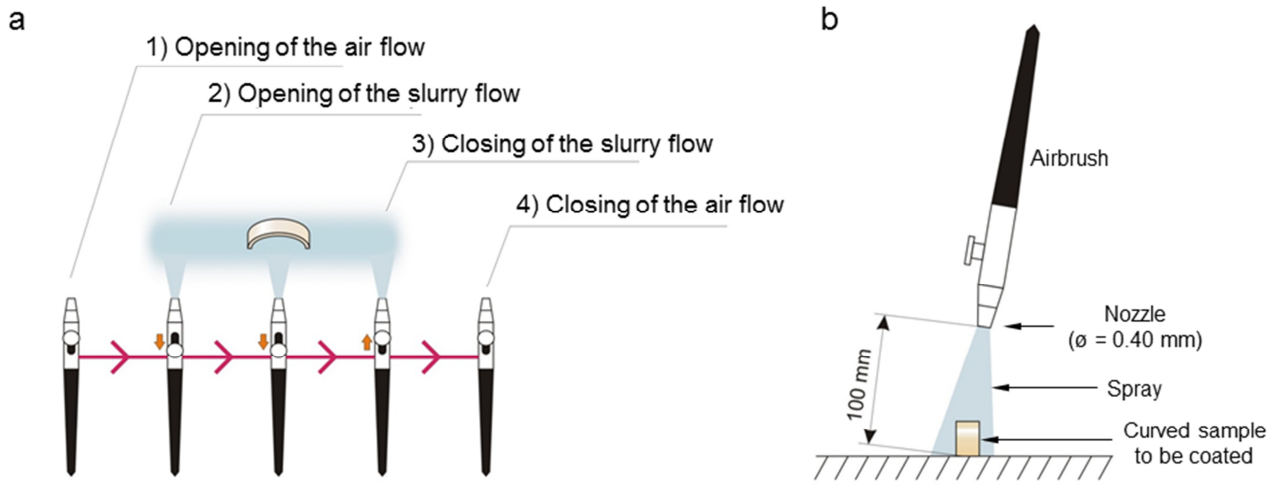
a
1) Opening of the air flow
2) Opening of the slurry flow
3) Closing of the slurry flow
4) Closing of the air flow
b
Airbrush
Nozzle
(ø = 0.40 mm)
100 mm
Spray
Curved sample
to be coated

Fig. 2

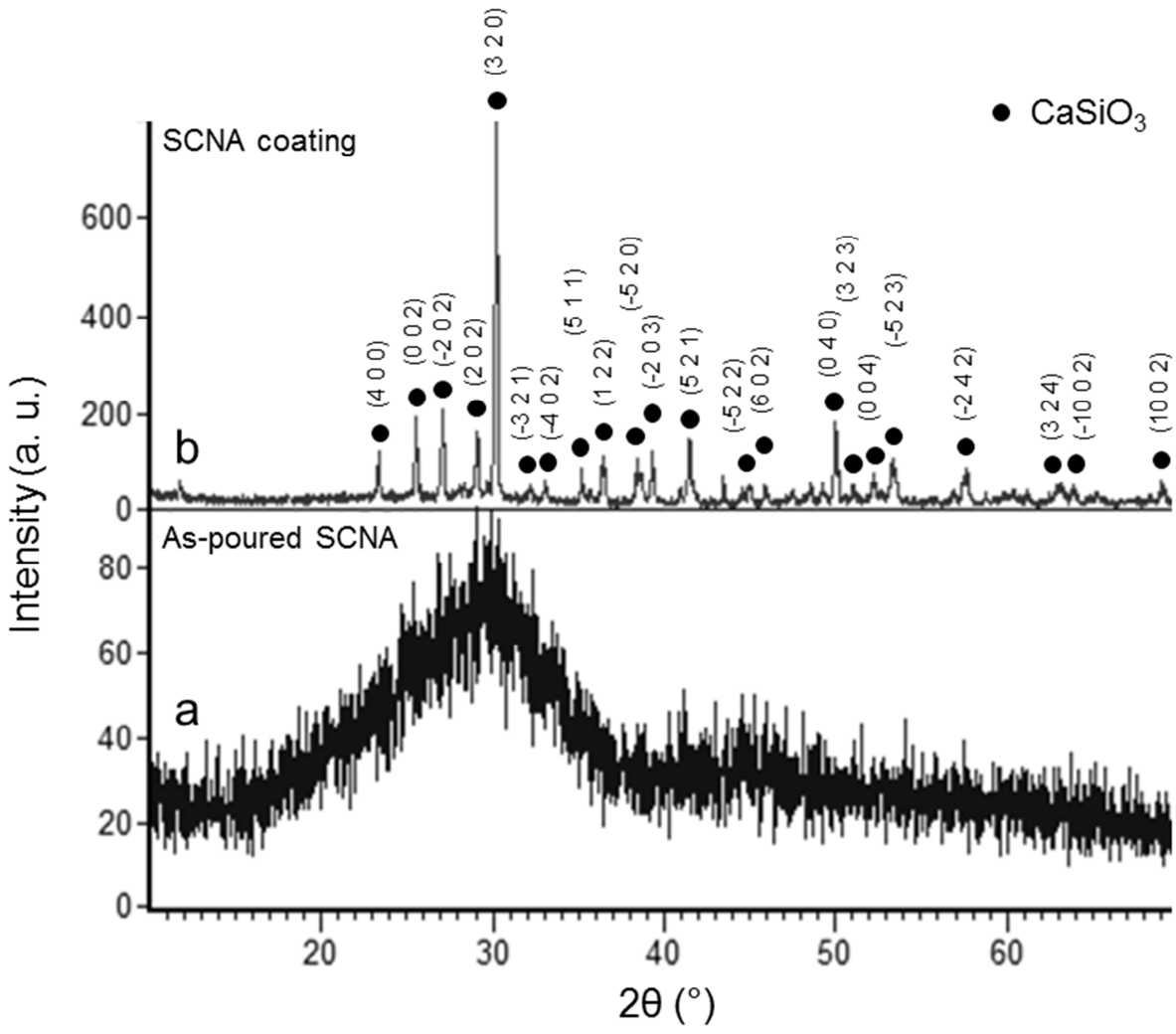
CaSiO3
SCNA coating
b
As-poured SCNA
a
Intensity (a. u.)
2θ (°)
(4 0 0)
(0 0 2)
(-2 0 2)
(2 0 2)
(3 2 0)
(-3 2 1)
(-4 0 2)
(5 1 1)
(1 2 2)
(-5 2 0)
(-2 0 3)
(5 2 1)
(-5 2 2)
(6 0 2)
(0 4 0)
(3 2 3)
(0 0 4)
(-5 2 3)
(-2 4 2)
(3 2 4)
(-10 0 2)
(10 0 2)

Fig. 3

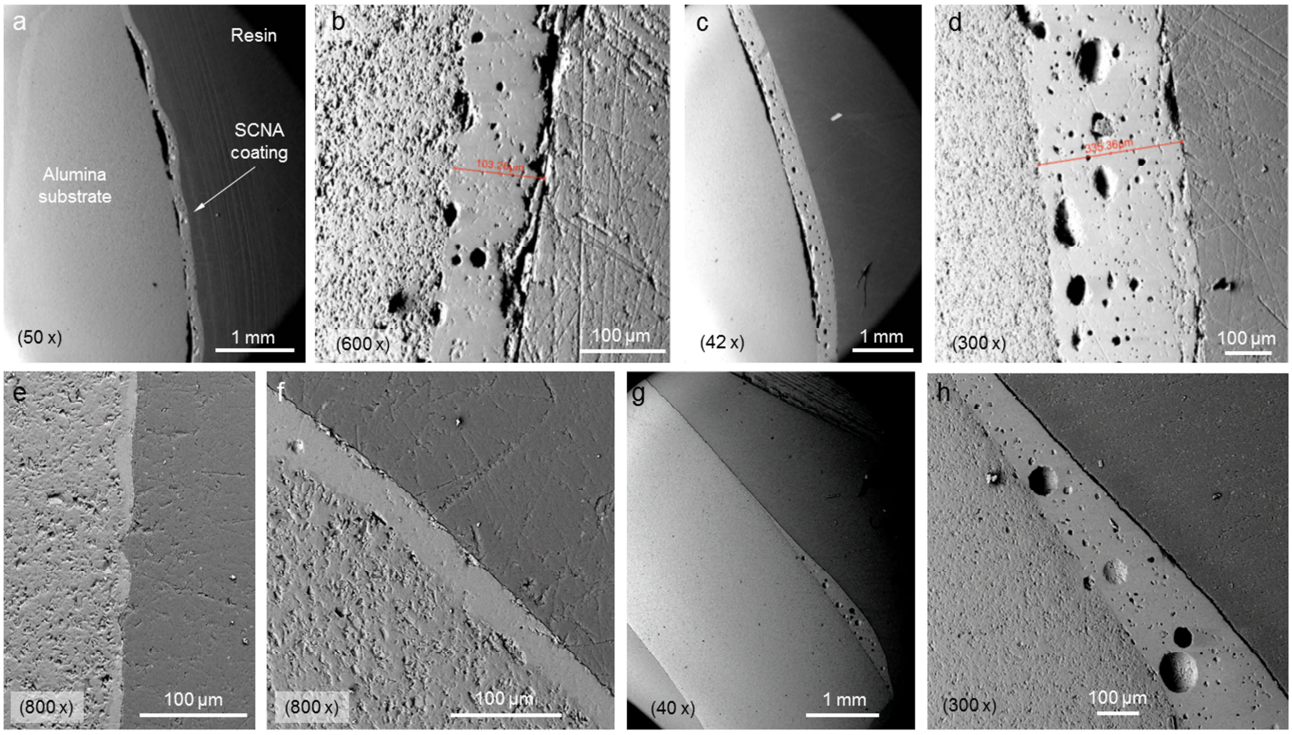
a
Resin
SCNA coating
Alumina substrate
(50 x)
1 mm
b
(600 x)
100 µm
c
(42 x)
1 mm
d
(300 x)
100 µm
e
(800 x)
100 µm
f
(800 x)
100 µm
g
(40 x)
1 mm
h
(300 x)
100 µm

Fig. 4

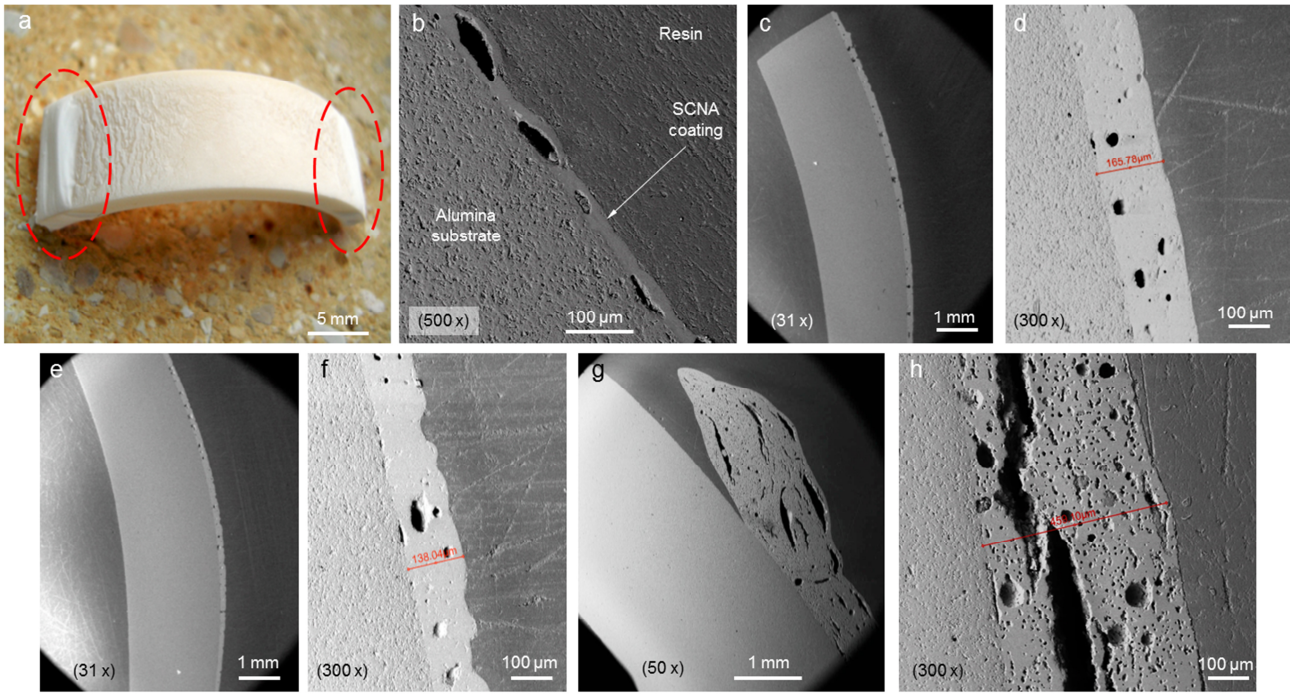
a
5 mm
b
Resin
SCNA coating
Alumina substrate
(500 x)
100 µm
c
(31 x)
1 mm
d
(300 x)
100 µm
e
(31 x)
1 mm
f
(300 x)
100 µm
g
(50 x)
1 mm
h
(300 x)
100 µm

Fig. 5

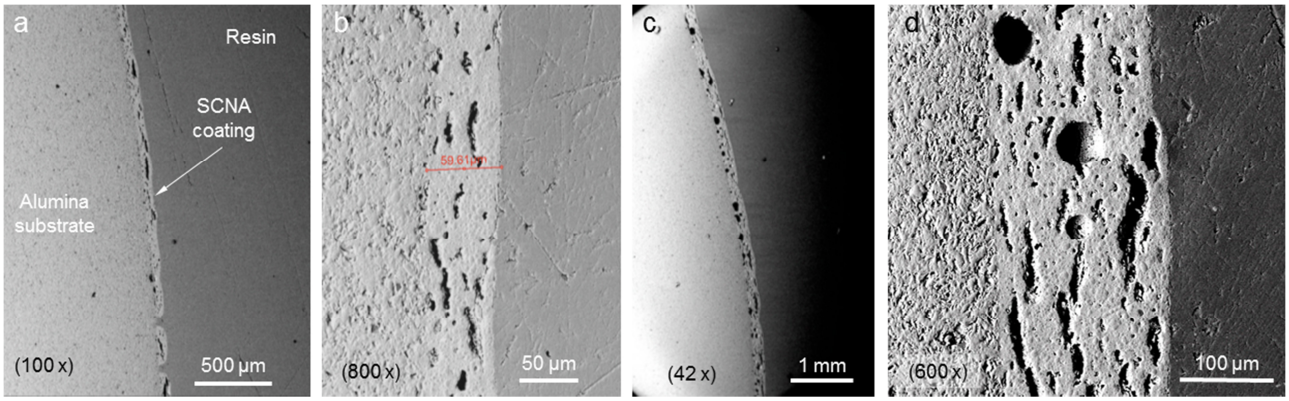
a
Resin
SCNA
coating
Alumina
substrate
(100 x)
500 µm
b
(800 x)
50 µm
c
(42 x)
1 mm
d
(600 x)
100 µm

Fig. 6

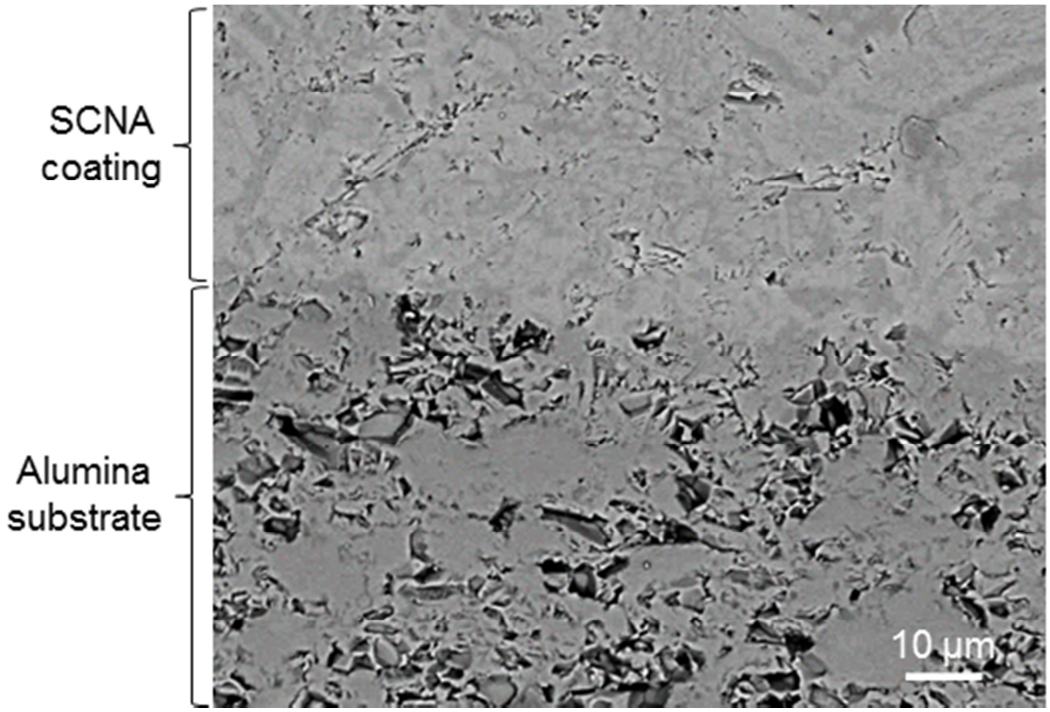
SCNA
coating
Alumina
substrate
10 µm

Fig. 7

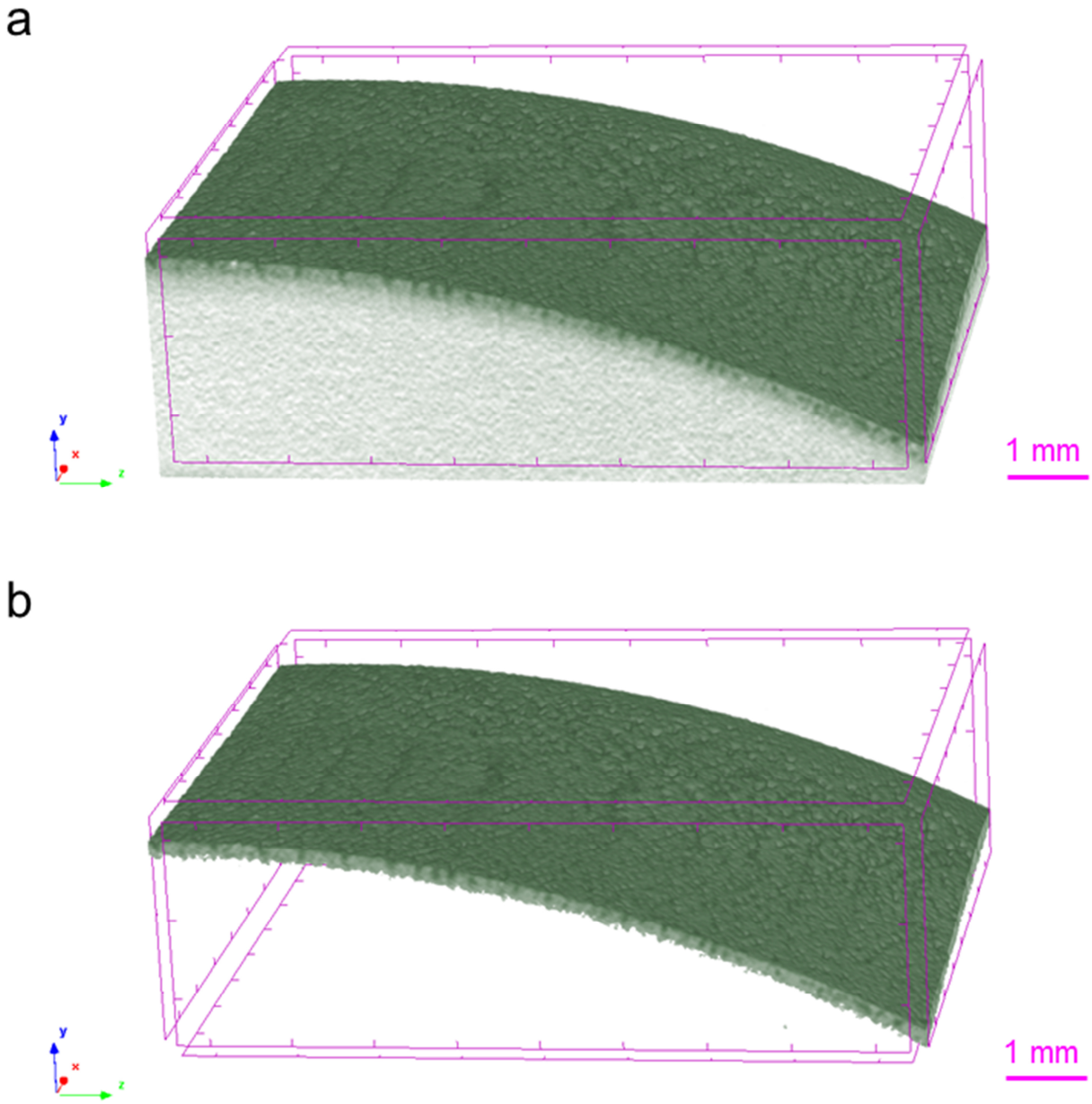

Fig. 8

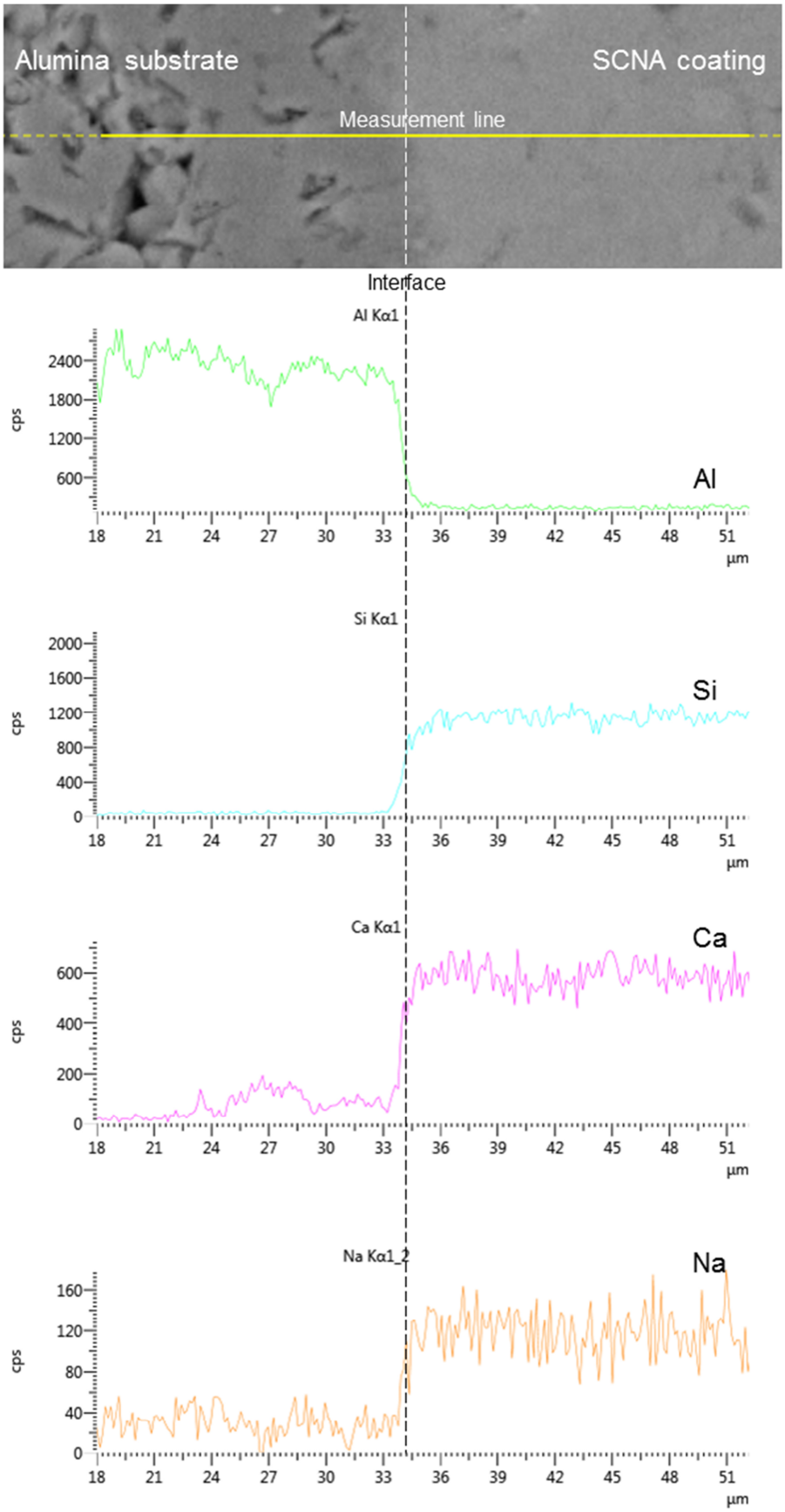
Alumina substrate
SCNA coating
Measurement line
Interface
Al Kα1
Al
Si Kα1
Si
Ca Kα1
Ca
Na Kα1_2
Na
cps
µm

Fig. 9

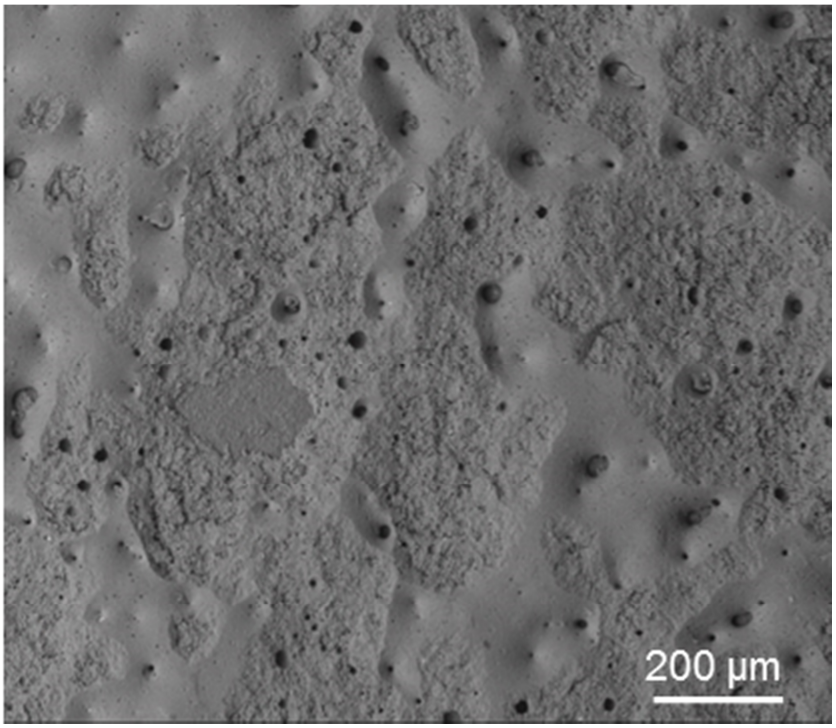
200 µm

Fig. 10

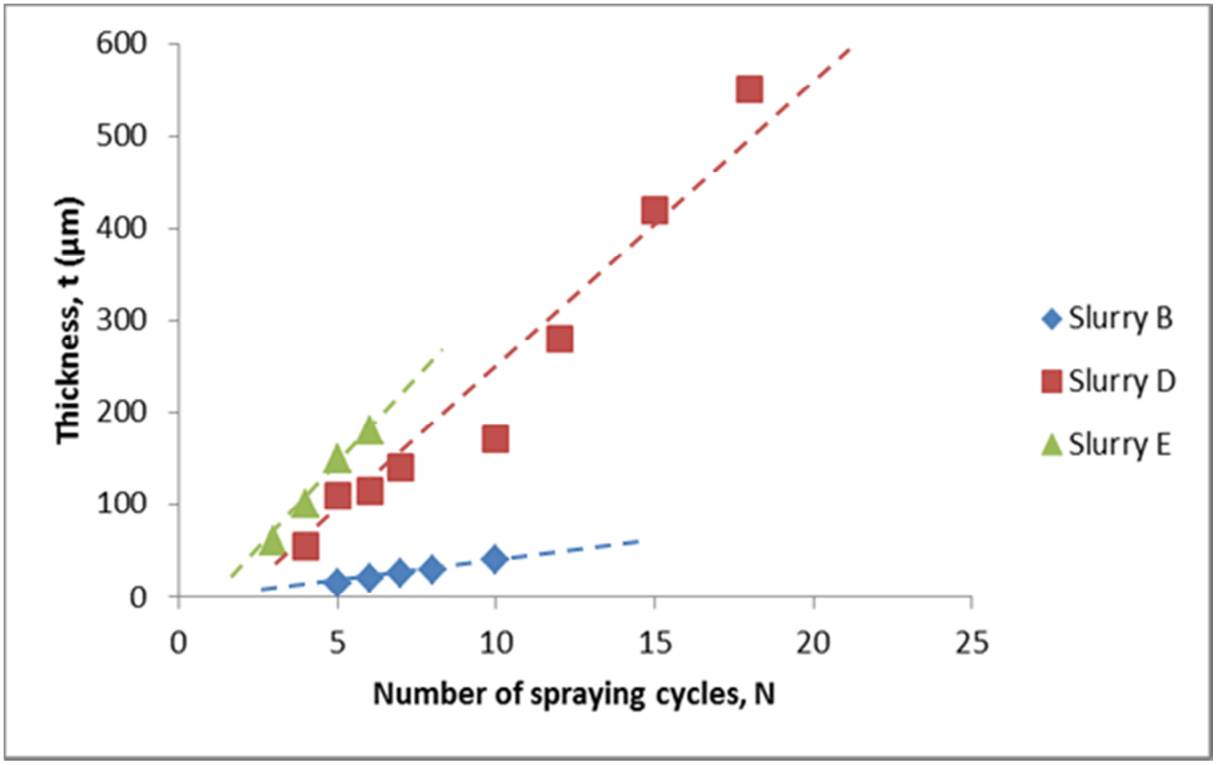
600
500
400
300
200
100
0
Thickness, t (µm)
0
5
10
15
20
25
Number of spraying cycles, N
Slurry B
Slurry D
Slurry E

Fig. 11